Band gap engineered Nb_2O_5 thin films fabricated from sol-gel processed modified precursors for enhanced photocatalytic activity: A comparative study

Mohammad Danish[1,2]*, Ashutosh Pandey[2]

[1]*Department of Chemistry, Periyar Maniammai University, Vallam, Thanjavur, 613403, India*
[2]*Department of Chemistry, Motilal Nehru National Institute of Technology, Allahabad, 211004, India*

*Corresponding author

DOI: 10.5185/amp.2018/846
www.vbripress.com/amp

Abstract

Reactions of niobium (V) ethoxide (**1**) with 2,4-pentanedione derivatives [3-Chloro-2,4-pentanedione, 1,1,1-Trifluoro-2, 4 pentanedione, 3,3-Dimethyl-2,4-pentanedione,] afforded heteroleptic niobium alkoxide complexes $[Nb(OEt)_4(CH_3COCHClCOCH_3)]$(**2**), $[Nb(OEt)_4(CF_3COCH_2COCH_3)]$ (**3**) and $[Nb(OEt)_4(CH_3COC(CH_3)_2COCH_3)]$ (**4**). Two sets of Nb_2O_5 sculptured thin films (STFs) were deposited on ITO coated glass substrates by spin casting the gels obtained by sol gel processing of the synthesized complexes (**2**-**4**). One set of the films (**Na, Nb** and **Nc**) were calcined under ammonia gas flow and the other (**a, b** and **c**) under oxygen gas flow respectively at 500°C for 1h. A film (**d)** was also fabricated from niobium (V) ethoxide and calcined under oxygen gas flow at 500°C for 1h for comparisons with regard to structure, topography, optical and photocatalytic properties of Nb_2O_5. Crystal structure, topography, optical and photocatalytic properties of the films were determined by X-ray diffraction, atomic force microscopy, ellipsometry and UV-Vis spectroscopy. Significant band gap narrowing i.e. from 3.48 eV (**d**) to 2.73 eV (**Nc**) was observed for the films calcined under ammonia gas flux. Investigation of photodegradation of methylene blue (MB) by niobia films under UV irradiation demonstrated enhanced degradation efficiency of methylene blue dye. Copyright © 2018 VBRI Press.

Keywords: Nb_2O_5 thin films, 2,4-pentanedione derivatives precursors, calcination under ammonia flow, optical properties, photocatalytic degradation.

Introduction

Niobium pentoxide because of its exclusive physical and chemical properties such as high refractive index, wide band gap, corrosion resistance and exceptional chemical stability [1-3] has emerged as one of the most important transition metal oxide in the recent years. As a consequence, it is being used in several modern technologies e.g. electrochromic devices [4, 5], gas sensors [6, 7], photocatalysts [8-11], photoelectrodes [7] and optoelectronic materials [12, 13]. In recent years, photo-degradation of organic molecules present in wastewater via aerobic oxidation using semiconductor photocatalysts has attracted a great deal of attention [9-11]. The exceptional efficiency of Nb_2O_5 in photocatalytic studies is attributed to its high energy band diagram (E_g =3.4 eV), crystal phases and morphological features. Specifically, nanostructured sol-gel derived Nb_2O_5 thin films offer high surface to volume ratios and quantum confinement effects that enable unique physical and chemical interactions to occur at the surface leading to enhanced efficiencies that are not seen in its bulk and powdered forms [14]. These films also have practical advantages of economical efficiency, environmental compatibility, reusability and durability in comparison to their nanoparticulate counterparts [15].

Although several film deposition techniques have recently been developed but sol-gel process emerges as a relatively simple, versatile and inexpensive deposition method. Besides, it allows control of the microstructure of the coating and produces durable and chemically stable films. The essence of the sol–gel technique is the transformation of molecular precursors into an oxide network by hydrolysis and condensation reactions [16]. Moreover, for fabrication of Nb_2O_5 thin films via sol-gel the most popular precursor in use is niobium (V) ethoxide $[Nb_2(OEt)_{10}]$ [17-18]. It exists as a dimer in solution state to attain octahedral coordination at Nb (V) centers via two bridging alkoxy ligands $[Nb_2(OR)_8(\mu\text{-}OR)_2]$ [19,20]. The presence of high number of facile alkoxy groups makes the complex highly susceptible to hydrolysis followed by a slow rate of polycondensation. Since, in the sol-gel process lowering of the rate of hydrolysis of the precursor is the most important factor for the formation of homogenous materials therefore controlled hydrolysis has been achieved by increasing the steric resistance of the alkoxy groups. It has been established that the rate of hydrolysis of Niobium (V) alkoxides, in general is lower

when alkyl chain length of the alkoxy group is longer or when the alkyl group is secondary or tertiary [21]. Since, increasing the chain length of alkoxy group involves complicated reactions, thus an alternate approach for controlling the rate of hydrolysis of highly reactive metal alkoxides (for example niobium (V) ethoxide) via substitution of some alkoxy groups by nucleophilic reagents like β-diketones, organic acids and glycols [22-27] had been successfully established. These ligands occupy some of the coordination sites of the central metal atom through less hydrophilic bonds or they impose other physical impedances such as steric effect to efficiently hinder the substitution of alkoxy group by hydroxyl group. Although, these ligands does not completely prevent the hydrolysis of the sites occupied by remaining alkoxy groups but effectively reduce the rate of hydrolysis [24]. The films obtained from gels prepared under controlled hydrolysis significantly influences optical and photocatalytic properties of Nb_2O_5 STFs.

One of the major problems faced during the photodegradation of pollutants in wastewater using nanostructured Nb_2O_5 as catalyst is its wide band gap which makes it inactive in visible light. Non-metal doping especially nitrogen doping has rapidly gained popularity among resarchers due to its cost-effectivness, eco-friendliness and comfortable handling. Thin films obtained by sol-gel methods are of much importance because of their microporous structure due to which significant incorporation and distribution of nitrogen throughout the film is possible [28]. Incorporation of nitrogen result in the mixing of N (*2p*) and O (*2p*) orbitals to form a valance band of higher negative potential leading to narrowing in the band gap [29-36]. The present work reports a comparative investigation of structural, topographical, optical and photocatalytic properties of sol-gel derived niobia thin films sculptured from the gels of novel heteroleptic niobium (V) complexes $[Nb(OEt)_4(CH_3COCHClCOCH_3)]$ (**2**), $[Nb(OEt)_4(CF_3COCH_2COCH_3)]$ (**3**) and $[Nb(OEt)_4(CH_3COC(CH_3)_2COCH_3)]$ (**4**) synthesized via nucleophilic substitution of niobium (V) ethoxide (**1**) with 3-Chloro-2,4-pentanedione, 1,1,1-Trifluoro-2,4 pentanedione, 3,3-Dimethyl-2,4-pentanedione, respectively. To best of our knowledge, so far, there is no detailed report on the fabrication and comparative analysis of Nb_2O_5 thin films from the systematically derived precursors or on the effects of calcination of the above said films under ammonia gas flow at 500 ºC.

Experimental

Preparation of Complexes

Niobium (V) ethoxide (**1**), 3-Chloro-2,4-pentanedione, 1,1,1-Trifluoro-2,4 pentanedione and 3,3-Dimethyl-2, 4-pentanedione, were purchased from Sigma Aldrich and used with no further purification. All reactions were carried out under a dry argon atmosphere by using standard Schlenk techniques. All solvents were dried and degassed prior to use.

$[Nb(OCH_2CH_3)_4(CH_3COCHClCOCH_3)]$ (**2**). 3-Chloro-2,4-pentanedione (1.5 mM) was slowly added to a solution of $Nb(OEt)_5$ (1.5 mM) in toluene (5ml) with constant stirring. The mixture was stirred for 12 h and the solvent was removed in vacuo to give a yellow liquid in 85% yield. ^{1}H NMR ($CDCl_3$) (25°C) δ 1.18 (t, C*H*$_3$CH$_2$O), 1.21 (t, C*H*$_3$CH$_2$O), 1.33 (t, C*H*$_3$CH$_2$O); 2.35 (s, C*H*$_3$CO), 3.81 (q, CH$_3$C*H*$_2$O), 4.11 (q, CH$_3$C*H*$_2$O), 4.23 (q, CH$_3$C*H*$_2$O).^{13}CNMR (25°C) δ 16.87 (*C*H$_3$CH$_2$O), 17.10 (*C*H$_3$CH$_2$O), 17.40 (*C*H$_3$CH$_2$O), 29.94 (OC*C*H$_3$), 66.26 (O*C*H$_2$CH$_3$), 70.16 (O*C*H$_2$CH$_3$), 70.28 (O*C*H$_2$CH$_3$), 91.21 (OC*C*HClCO), 191.60 (O*C*CH$_3$). Elem. anal. for $[Nb(OCH_2CH_3)_4(CH_3COCHClCOCH_3)]$ *calc*. C = 38.30, H = 6.67 and *exp*. C = 37.96 and H = 6.24.

$[Nb(OCH_2CH_3)_4(CF_3COCH_2COCH_3)]$ (**3**). 1,1,1-Trifluoro-2,4-pentanedione (1.5 mmoles) was slowly added to a solution of $Nb(OEt)_5$ (1.5 mmoles) in toluene (5ml) with constant stirring. The mixture was stirred for 12 h and the solvent was removed in vacuo to give a light yellow liquid in 86% yield. ^{1}H NMR ($CDCl_3$) (25°C) δ 1.09 (t, C*H*$_3$CH$_2$O), 1.21 (t, C*H*$_3$CH$_2$O), 1.34 (t, C*H*$_3$CH$_2$O); 2.56 (s, C*H*$_3$CO), 3.72 (q, CH$_3$C*H*$_2$O), 4.11 (q, CH$_3$C*H*$_2$O), 4.62 (q, CH$_3$C*H*$_2$O), 6.02 (s, COC*H*$_2$CO); ^{13}CNMR (25°C) δ 16.87 (*C*H$_3$CH$_2$O), 16.93 (*C*H$_3$CH$_2$O), 17.30 (*C*H$_3$CH$_2$O), 27.94 (OC*C*H$_3$), 65.26 (O*C*H$_2$CH$_3$), 69.26 (O*C*H$_2$CH$_3$), 69.38 (O*C*H$_2$CH$_3$), 97.61 (OC*C*HCO), 118.75 (q, *C*F$_3$), 169.38 (q, OC*C*F$_3$), 186.37 (O*C*CH$_3$). Elem. anal. for $[Nb(OCH_2CH_3)_4(CF_3COCH_2COCH_3)]$ *calc*. C = 36.37, H = 6.34 and *exp*. C = 35.86 and H = 5.12.

$[Nb(OCH_2CH_3)_4(CH_3COC(CH_3)_2COCH_3)]$ (**4**). 3, 3-Dimethyl-2,4-pentanedione (1.5 mM) was slowly added to a solution of $Nb(OEt)_5$ (1.5 mM) in toluene (5ml) with constant stirring. The mixture was stirred for 12 h and the solvent was removed in vacuo to give a colorless liquid in 90% yield. ^{1}H NMR ($CDCl_3$) (25°C) δ 1.14 (t, C*H*$_3$CH$_2$O), 1.19 (t, C*H*$_3$CH$_2$O), 1.29 (t, C*H*$_3$CH$_2$O); 2.28 (s, C*H*$_3$CO), 3.90 (q, CH$_3$C*H*$_2$O), 4.09 (q, CH$_3$C*H*$_2$O), 4.51 (q, CH$_3$C*H*$_2$O), 5.22 (s, COC(C*H*$_3$)$_2$CO). ^{13}CNMR (25°C) δ 15.81 (*C*H$_3$CH$_2$O), 15.93 (*C*H$_3$CH$_2$O), 16.10 (*C*H$_3$CH$_2$O), 23.09 [OCC(*C*H$_3$)$_2$CO], 30.52 (OC*C*H$_3$), 65.26 (O*C*H$_2$CH$_3$), 69.16 (O*C*H$_2$CH$_3$), 69.28 (O*C*H$_2$CH$_3$), 89.61 [OC*C*(CH$_3$)$_2$CO], 186.60 (O*C*CH$_3$). Elem. anal. for $[Nb(OCH_2CH_3)_4(CH_3COC(CH_3)_2COCH_3)]$ *calc.* C = 44.89, H = 8.04 and *exp*. C = 43.86 and H = 7.62.

Fabrication of Nb_2O_5 sculptured thin films

Nb_2O_5 sol was prepared by dissolving the precursor alkoxide [**1**, **2**, **3** and **4**] (1.0 mM) in ethanol (3 ml) with constant stirring for 3h. Deionized water (1ml) was added to the resultant clear sol under vigourous stirring to obtain the gel. The resultant homogenous gel was spin casted onto ITO coated glass substrate at 1500 rpm for 60 sec. The spin casting procedure was repeated once again to obtain films with uniform thickness. One set of films so formed respectively from complex 2 (**a**), complex 3 (**b**), complex 4 (**c**) and $Nb(OEt)_5$ (**d**) were calcined under oxygen gas (40 ml/min) flow, while the other set of the films (**Na**, **Nb** and **Nc**) were calcined under ammonia gas

flow (40 ml/min) at 500 ºC for 1h. The films so formed were found to be stable for more than two months.

Photocatalytic degradation of methylene blue dye

The photocatalytic degradation of methylene blue (MB) by Nb_2O_5 STFs over a period of 480 minutes at ambient temperature and pressure was investigated. The film was immersed in 50 ml of MB solution (4mg/L). The reactor was equipped with a 300 W high-pressure mercury UV tube emitting near UV radiation with a peak wavelength of 365 nm. Factors like dye concentration, pH, temperature etc. were kept constant in all the experiments. The distance between the light source and film was kept constant to achieve a constant light intensity on the film surface. The photocatalytic degradation of MB was monitored by measuring the absorbance of the solution with a UV–Vis spectrophotometer.

Characterization

^{1}H NMR spectra and ^{13}C NMR spectra were recorded using a Bruker Advance II 400 MHz NMR spectrometer and are referenced to TMS. FT-IR spectra were recorded using Perkin Elmer FT-IR spectrophotometer.The crystal structures of the Nb_2O_5 films were determined by X-ray diffractometer (Rigaku Smartlab, Japan) operated at 40 kV, 30 mA. Cu Kα (λ = 1.541 78 Å) was used at X-Ray source. Topographical features of the films were investigated with AFM (Agilent technologies). The optical constants and thickness of the films were characterized using variable angle spectroscopic ellipsometer (VASE J.A. Woollam Co., Inc) at wavelengths ranging from 300 nm to 1000 nm. Transmittance was recorded using UV-Vis spectrophotometer (Shimadzu-UV 3600 plus) along a range of wavelengths from 300 nm to 1400 nm. Absorption coefficient (α) was calculated using the equation.

$$\alpha = 1/d \ln (1/T) \quad (1)$$

where d and T respectively represents the thickness and transmittance of films [39].

Results and discussion

The reaction of niobium (V) ethoxide (**1**), with the used β-diketone derivative in 1:1 molar ratio, giving products [Nb(OEt)$_4$[β-diketonate] **2-4** in good yields. The IR spectrum of each compound showed bands at $\upsilon \approx 1670$ cm^{-1} and 1556 cm^{-1} indicating the presence of CO and CH groups of β-diketonate ligands. Bands in the range of $\upsilon \approx 500$ cm^{-1} to 900 cm^{-1} are assigned to Nb-O stretching and Nb-O-Nb vibrations.

The ^{1}H NMR of compound **4** shows three sets of triplet (δ 1.09, 1.21 and 1.34) and quartet (δ 3.72, 4.11 and 4.62) suggesting that in solution the molecule contains OEt ligands in three types of environments in an intensity ratio of 2:1:1. Singlets at δ 2.56 and 6.02 respectively are indicative of the methyl and methine protons of the β-diketonate ligand. Similarly, ^{1}H NMR spectra of all other compounds also demonstrate octahedral structure for the precursor complexes.

Nb_2O_5 STFs of uniform thicknesses were obtained using sol-gel technique. Spin coating at 1500 rpm for 60 sec yielded ≈ 200 nm thick films. The thickness of ITO coated glass substrate was 3 mm and thickness of ITO coating was determined to be 120 nm.

Crystal structures and topography of Nb_2O_5 STFs

Crystal structures of the films were investigated by X-ray diffraction **(Fig 1.)**. It can be observed that film **d** crystallizes into metastable hexagonal Nb_2O_5 (JCPDS card No. 7-61) [37] phase confirmed by peaks at (2θ); 22.58, 28.76, 36.81, 46.17, 50.68 and 55.33 and average crystallite size of 21.4 nm. No obvious peaks were identified on the XRD patterns of **a**, **b**, **c**, **Na**, **Nb** and **Nc** indicating their amorohous nature. However, film **c** show the transformation of phase from metastable hexagonal to stable monoclinic phase confirmed by the presence of peaks at (2θ) 25.17 and 48.02 (JCPDS Card No. 00-019-086) [38].

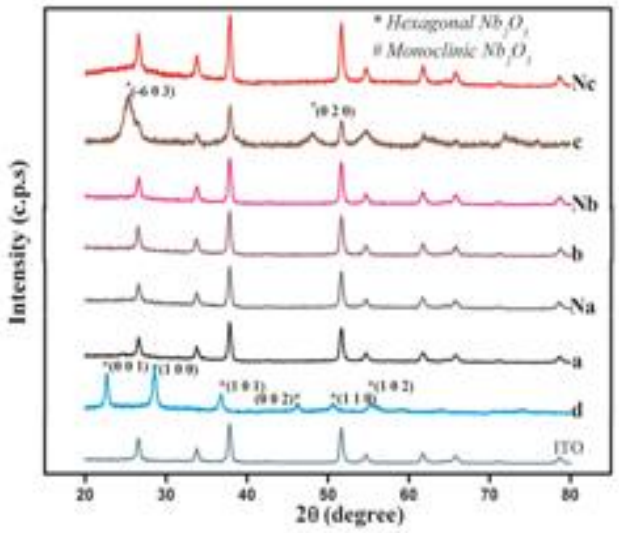

Fig. 1. XRD patterns of Nb_2O_5 thin films **a**, **Na** fabricated from complex **2**; **b**, **Nb** from complex **3**; **c**, **Nc** from complex **4**; **d** from **1** and calcined under oxygen/ammonia gas flow for 500 °C for 1h.

The diffraction patterns evidently colligate a transformation of phase from hexagonal to thermodynamically more stable monoclinic phase of Nb_2O_5 crystallites on modification of Nb(OEt)$_5$ to Nb(OEt)$_4$(β-diketonate). This further substantiates the existence of structure property relationship between the precursor and the final metal oxide film in the sol-gel process. The observed trends in the XRD patterns are believed to be the result of slower rate of hydrolysis. The hindrance in hydrolysis by steric effects is expected to be more pronounced in the modified niobium (V) ethoxide complexes. As the hydrolysis of the alkoxide is followed by polymerization and condensation processes which determine the structure of gels and subsequently the structure of the films. Based on the obtained XRD patterns it may be concluded that the rate of hydrolysis is

hindered to an extent so that only small oligomeric units were formed leading to the elevation of crystallization process to a higher temperature in films **a** and **b** fabricated from modified complexes **1** and **2**. However, interestingly the rate of hydrolysis in complex **3** is believed to be faster as compared to complexes **1**and **2** causing an extensive cross-linking leading to stabilized monoclinic Nb_2O_5 crystallites on film **c** with average crystallite size of 18.1 nm.

The reaction of ammonia with films at 500 °C for 1h leads to the elevation of crystallization process to higher temperature as compared to oxygen-calcined films. This is due to the incorporation of nitrogen in the lattice sites of mesoporous niobia films which is an established crystallization inhibitor [31]. This is further evidenced by the average crystallite sizes **(Table 1)** of Nb_2O_5 on the various films as calculated by Debye Scherrer equation.

Table 1. Average crystallite sizes, RMS roughnesses, refractive indices (n), extinction coefficients (k), band gap energies (E_g) and percent degradation of MB dye for Nb_2O_5 thin films fabricated from $Nb(OEt)_5$ (**1**) and systematically synthesized $Nb(OEt)_4$(ß-diketonates) complexes (**2-4**).

Sample	Average crystallite size (nm)	RMS Roughness (nm)	Refractive Index (n) at 550 nm	Extinction coefficient (k) at 550 nm	Band gap energy [E_g] (eV)	Degradation of MB (%)
a	---	2.34	2.58	0.0833	3.38	70.12
b	---	2.09	2.52	0.0773	3.36	73.12
c	18.105	2.75	2.78	0.0000	3.60	61.13
Na	---	1.39	2.32	0.0632	2.93	81.72
Nb	---	1.08	2.39	0.0675	3.32	78.14
Nc	---	0.94	2.24	0.0997	2.73	88.16
d	21.42	3.59	3.18	0.0000	3.48	62.13

AFM micrographs of the films are illustrated in **Fig. 2.** The images show non-compact morphologies of the deposited Nb_2O_5 thin films and the absence of cracks. RMS surface roughnesses are tabulated in **Table 1**. The micrographs clearly show that surface roughness of films increases as a function of crystallite size of Nb_2O_5 nanocrystallites. However, the films fabricated from the gels of modified niobium (V) ethoxide complexes were found to be smoother than the films fabricated from the parent alkoxide. It is believed that nucleophilic substitution of ethoxy group of niobium (V) ethoxide precursor by substituted 2,4-pantanedione derivatives, reduced the rate of hydrolysis and thus extent of cross-linking resulting in easier relaxation of polymer strands. Consequentially, the fabrication of stable, continuous and smoother films is facilitated. Also the RMS roughness of ammonia-calcined films was observed to significantly lower than that of oxygen calcined films. The lowering of surface roughness of films on treatment with ammonia at 500 °C may once again be attributed to the incorporation of nitrogen leading to the elevation of crystallization process to a higher temperature and hence smoother surface.

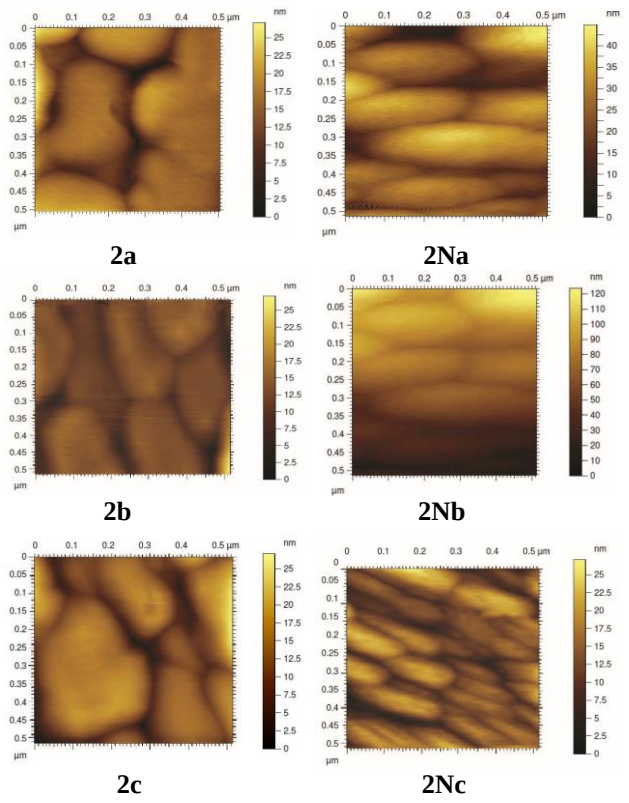

Fig 2. 2D AFM surface images of Nb_2O_5 thin films Nb_2O_5 thin films **a**, **Na** fabricated from complex **2**; **b**, **Nb** from complex **3**; **c**, **Nc** from complex **4**; **d** from **1** and calcined under oxygen/ammonia gas flow for 500 °C for 1h.

Optical properties of Nb_2O_5 thin films

Refractive indices (n) and extinction coefficients (k) of Nb_2O_5 thin films were obtained from variable angle spectroscopic ellipsometry measurements and listed in **Table 1**. Tauc-Lorentz oscillator model was used to determine the physical parameters based on the choice of best model that enables good fitting results of theoretical curves of cos (Δ) and tan (Ψ) to experimental ones as a function of the wavelength [36]. As shown in **Fig. 3,** refractive indices (n) of films **a**, **b** and **c** ranged from 2.52 to 2.78 while **d** exhibited a higher value of 3.18.

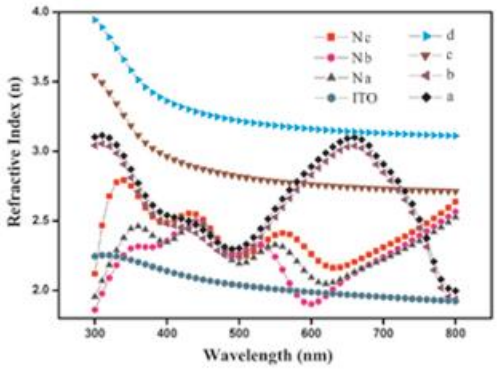

Fig. 3. Refractive indices (n) of Nb_2O_5 thin films Nb_2O_5 thin films **a**, **Na** fabricated from complex **2**; **b**, **Nb** from complex **3**; **c**, **Nc** from complex **4**; **d** from parent complex **1** and calcined under oxygen/ammonia gas flow for 500 °C for 1h.

This observation may be ascribed to the disparity in crystallinity, crystal structure and packing density of Nb_2O_5 crystallites on the films generated as a result of different rates of hydrolysis of the precursor complexes. This leads to different extent of cross-linking of units and hence, difference in crystallization processes and crystallization temperature can be explained. The n values for films **Na**, **Nb** and **Nc** ranged from 2.24 to 2.39. Interestingly, refractive indices of ammonia-calcined thin films decreases comprehensively as compared to those of oxygen calcined films. The observation can be explained again on the basis of elevated crystallization restricted rate of nucleation upon incorporation of nitrogen and hence, decreased packing density. This further validates the incorporation of nitrogen on the surface of films. The extinction coefficient (k) values for all the films were found to be in the range of 0.000 to 0.099 at 550 nm, exhibiting minimum loss of electromagnetic radiation.

Fig. 4 illustrates the obtained optical transmittance (T) of films. The deposited films were highly transparent in the measured spectral range from 300 nm to 1400 nm. A sharp rise in transmittance was observed up to 50% for all films. However, for films **a**, **c** and **d** this sharp rise continued up to 77% forming transmission edge in UV region. Transmittance for all the films remained in the range of 60% to 80% in visible region. Notably, red shift in the wavelength of transmission edge was observed with decrease in crystallinity of niobia on films. This may be attributed to difference in surface morphologies, crystallite sizes, higher packing densities and existence of surface defects causing a decrease in transmittance and shift of λ_{max} due to scattering of light.

The band gap energy of all films was quantitatively determined from Tauc equation corresponding to direct gap n-type semiconductors. The $(\alpha h\upsilon)^2$ versus photon energy (E_g) plot **(Fig. 5)** gave an estimate of the band gap energy of thin films tabulated in table 1. The plot exhibits lowering of band gap energy for oxygen-calcined films fabricated from complexes **2** and **3**. However, high band gap energy was found for film fabricated from complex **4** and parent niobium (V) ethoxide. The observation clearly suggests the lowering of E_g on substitution of nucleophilic β-diketone moiety in niobium (V) ethoxide.

Band gap narrowing upon modification of niobium (V) is believed to be the result of steric impedance offered to hydrolysis of the synthesized precursors leading to different extent of cross-linking matrix formation and hence affecting the band gap of Nb_2O_5 nanocrystallites accordingly. Accordingly, from the observations it can be established that the rate of hydrolysis is faster in complex **3** leading to the formation of short cross-linked matrix as compared to those of complexes **1** and **2**. As a result Nb_2O_5 nanocrystallites on film **c** fabricated from complex 3 is more crystalline leading to high band gap as compared to films **a** and **b**.

Interestingly, comprehensive narrowing of band gap energy was observed for ammonia-calcined thin films **Na**, **Nb** and **Nc** (2.94 eV, 2.73 eV and 3.33 eV respectively) as compared to those calcined under oxygen gas flow. This further establishes the incorporation of nitrogen on the surface of mesoporous Nb_2O_5 thin films.

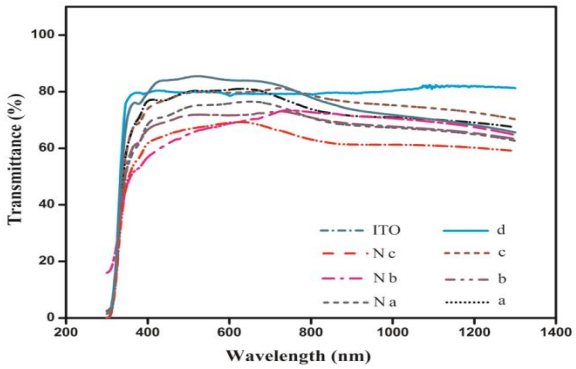

Fig. 4. The optical transmittance of Nb_2O_5 thin films **a**, **Na** fabricated from complex **2**; **b**, **Nb** from complex **3**; **c**, **Nc** from complex **4**; **d** from parent complex **1** and calcined under oxygen/ammonia gas flow for 500 °C for 1h.

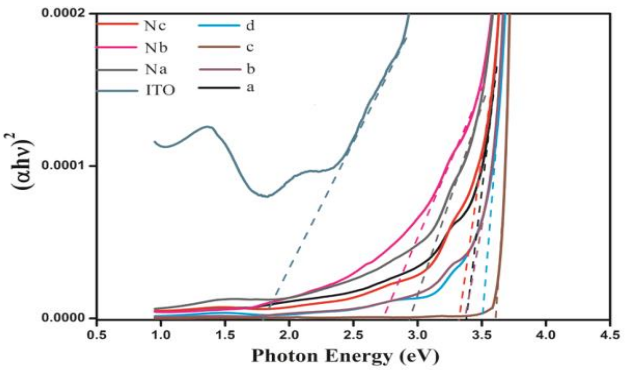

Fig. 5. Plot of $(\alpha h\upsilon)^2$ v/s photon energy (E_g) for Nb_2O_5 thin films **a**, **Na** fabricated from complex **2**; **b**, **Nb** from complex **3**; **c**, **Nc** from complex **4**; **d** from complex **1** and calcined under oxygen/ammonia gas flow for 500 °C for 1h.

Photocatalytic efficiency of Nb_2O_5 thin films

Fig. 6 exhibits the comparative percent degradation of MB dye for all Nb_2O_5 STFs. It is clear that film **Nb** showed best photocatalytic activity in the time limit of 480 mins. It degraded methylene blue up to 88.72% followed by **Na** and **Nc** (81.72% and 78.12% respectively). However, films (**a**, **b**, **c** and **d**) calcined under oxygen flux degraded only 70.12%, 73.22%, 61.23% and 62.13% respectively of MB.

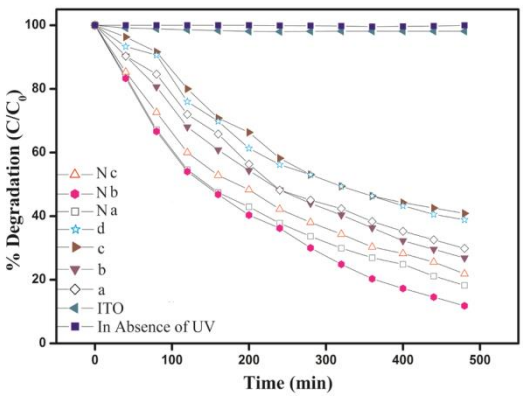

Fig. 6. Photocatalytic degradation of methylene blue by Nb_2O_5 thin films under UV light over a time period of 480 minutes.

The mechanism of photocatalysis involves the absorption of a photon with sufficient energy (equals or higher than the band-gap energy (E_g) of the catalyst) leading to a charge separation due to excitation of an electron (e^-) from the valence band of the semiconductor catalyst to the conduction band. Thus, generating a hole (h^+) in the valence band [40].

The recombination of the electron and the hole must be prevented for the photon induced catalysis reaction to proceed. The photogenerated electrons could reduce the dye or react with electron acceptors such as O_2 adsorbed on the semiconductor surface or dissolved in water, reducing it to superoxide radical anion $O_2^{-\bullet}$ [41]. The photogenerated holes can oxidize the organic molecule to form R^+, or react with OH^- or H_2O oxidizing them into $^\bullet OH$ radicals. In general, the proposed mechanism of photocatalysis at the semiconductor surface causing the degradation of dyes can be expressed as follows:

$$Nb_2O_5 + h\nu(UV) \rightarrow Nb_2O_5\ (eCB^- + hVB^+) \quad (\mathbf{3})$$

$$Nb_2O_5\ (hVB^+) + H_2O \rightarrow Nb_2O_5 + H^+ + OH^\bullet \quad (\mathbf{4})$$

$$Nb_2O_5\ (hVB^+) + OH^- \rightarrow Nb_2O_5 + OH^\bullet \quad (\mathbf{5})$$

$$Nb_2O_5\ (eCB^-) + O_2 \rightarrow Nb_2O_5 + O_2^{-\bullet} \quad (\mathbf{6})$$

$$O_2^{-\bullet} + H^+ \rightarrow HO_2^\bullet \quad (\mathbf{7})$$

$$Dye + OH^\bullet \rightarrow \text{degradation products} \quad (\mathbf{8})$$

$$Dye + hVB^+ \rightarrow \text{oxidation products} \quad (\mathbf{9})$$

$$Dye + eCB^- \rightarrow \text{reduction products} \quad (\mathbf{10})$$

where hv is photon energy required to excite the semiconductor electron from the valence band (VB) region to conduction band (CB) region.

For the oxygen-calcined films, the difference in photocatalytic activities of the films can be attributed to the difference in crystallinity, crystallite size and band gap energy of niobia nanocrystallites on films. Generally, smaller grains results in a larger surface area, consequently increasing the number of the absorptive sites for the reaction. Moreover, a photon having energy greater than the band-gap energy of nanoparticles, transfers its energy to valance band electron, which is excited to conduction band leaving a hole in valance band. As the Nb_2O_5 crystallite size decreases, transmission of holes to the surface of catalyst increases and the probability of the recombination of electron-hole pairs decreases, resulting in an enhanced photocatalytic activity.

However, the enhanced performances of the films calcined under ammonia environment is believed to be a consequence of band gap narrowing upon incorporation of nitrogen in Nb_2O_5 lattice leading to increased number photogenerated electrons and holes created by the excitation of electrons and decreased rate of e^-/h^+ pair recombination leading to enhanced degradation of MB at the surface of Nb_2O_5 nanostructures film. Thus the observed photodegradation of MB establishes that photocatalytic activity of niobia films strongly depends on the band gap of the catalyst, which in this case had been engineered via chelating the parent alkoxide with nucleophilic ß-diketone ligands to controll the rate of hydrolysis and importantly by incorporation of nitrogen via calcinating the deposited films under flowing ammonia at 500 °C for 1h.

Conclusion

Synthesized tetraethoxo (β-diketonato) niobium (V) complexes $[Nb(OEt)_4(CH_3COCHClCOCH_3)]$ (**2**), $[Nb(OEt)_4(CF_3COCH_2COCH_3)]$ (**3**) and $[Nb(OEt)_4(CH_3COC(CH_3)_2COCH_3)]$ (**4**) were observed to be better precursor for the fabrication of stable, durable and crack-free Nb_2O_5 thin film via sol-gel than the parent alkoxide (**1**). Films **a**, **b**, **c** and **d** were calcined under oxygen gas flow while films **Na**, **Nb** and **Nc** were calcined under ammonia gas flow at 500 °C for 1h. Film **c** crystallizes into thermodynamically more stable monoclinic crystal structure with average crystallite size of 18.10 nm. While, structure of nanocrystallites on film (**d**) fabricated from niobium (V) ethoxide was observed to be hexagonal with size of 21.4 nm. Refractive indices and extinction coefficient values were found to in the range of 2.24 to 3.18 and 0.000 to 0.099 respectively. All the films were highly transparent (T≤ 80%) in the visible region with low reflectivity and hence these films can be potential candidates for antireflective applications. Reduction in band gap energy from 3.48 eV to 3.38 eV upon modification of $Nb(OEt)_5$ to $Nb(OEt)_4$(β-diketonate) was observed. However, significant narrowing of band gap energies from 3.60 eV to 2.73 eV was observed on calcining the films under ammonia gas flow. On the account of small crystallite size and reduced band gap energy the films were tested for photocatalytic degradation of methylene blue. Films fabricated from $Nb(OEt)_4$(β-diketonate) and calcined under ammonia gas flow exhibited greater degradation of MB than film sculptured from $Nb(OEt)_5$ and $Nb(OEt)_4$(β-diketonate) and calcined under oxygen gas flow. Maximum degradation of 88.72% was exhibited by thin film **Nb**, followed by **Na** and **Nc** (81.72% and 78.12% respectively) over the time period of 480 min. while, **a**, **b**, **c** and d degraded only 70.12%, 73.22%, 61.23% and 62.13% respectively.

Acknowledgements

The Authors are grateful to Centre for interdisciplinary research facility, MNNIT, Allahabad for the instrumentation facility.

Author's contributions

Conceived the plan: AP, MD; Performed the expeirments: MD; Data analysis: AP, MD; Wrote the paper: MD, AP. Authors have no competing financial interests.

References

1. Lazarova, K; Vasileva, M; Marinov, G; Babeva, T; Optics & Laser Technol, **2014**, 58, 114.
2. Zhao, Y; Zhou, X; Ye, L; Tsang, S.C.E; Nano Rev., **2012**, 3, 1763.
3. Agarwal, G; Reddy, G.B; J Mater Sci: Mater Electron, **2005**, 16, 21.
4. Livage, J; Ganguli, D; Sol. Energy Mater. Sol. Cells, **2001**, 68, 365.

5. Aegerter, M.A.; Avellaneda, C.O; Pawlicka, A; Atik, M; J. Sol–Gel Sci. Technol., **1997**, 8, 689.
6. Aegerter, M.A; Sol. Energy Mater. Sol. Cells, **2001**, 68, 401.
7. Wang, Y. –d; Yang, L.–f; Zhou, Z.–l; Li, Y.–f; Wu, X.H; Mater. Lett., **2001**, 49, 277.
8. Dhar, A.; Alford, T.L; J. Appl. Phys., **2012**, 112, 103.
9. Pai, Y.–h; Fang, S.-y; J. Power Sources, **2013**, 230, 321.
10. Qi, S; Zuo, R; Liu, Y; Wang, Y; Mater. Res. Bull., **2013**, 48, 1213.
11. Ge, S.; Jia, H; Zhao, H; Zheng, Z; Zhang, L; J. Mater. Chem., **2010**, 20, 3052.
12. Guo, S. –q; Zhang, X; Zhou, Z; Gao, G.–d; Liu, L; J. Mater. Chem. A, **2014**, 2, 9236.
13. Gandhi, J; Dangi, R; Bhardwaj, S; Rasayan. J. Chem., **2008**, 1, 567.
14. Guo, P; M.A. Aegerter, Thin Solid Films 351, 290 (1999)
15. Rani, R.A; Zoolfakar, A.S; O'Mullane, P.A; Austin, M.W; Zadeh, K.K; J. Mater. Chem. A, **2014**, 2, 15683.
16. Huang, Y; Xu, Y; Ding, S.J; Lu, H.L; Sun, Q.Q; Zhang, D.W; Chen, Z; Appl. Surface Sci., **2011**, 257, 7305.
17. Özer, N; Barretob, T; Büyüklimanlic, T; Lampert, C.M; Sol. Energy Mater. Sol. Cells, **1995**, 36, 433.
18. Lenzmann, F; Shklover, V; Brooks, K; Gratzel, M; J. Sol-Gel Sci. Technol., **2000**, 19, 175.
19. Özer, N; Rubin, M.D; Lampert, C.M; Sol. Energy Mater. Sol. Cells, **1996**, 40, 285.
20. Pollard, K.D; Puddephatt, R.J; Chem. Mater., **1999**, 11, 1069.
21. Narula, A.K; Singh, B; Kapoor, P.N; Kapoor, R.N; Synth. React. Inorg. Met.-Org. Chem., **1983**, 13, 887.
22. Mehrotra, R.C; Pure & Appl. Chem., **1988**, 60, 1349.
23. Mehrotra, R.C; Rai, A.K; Kapoor, P.N; Bohra, R; Inorg. Chim. Acta, **1976**, 16, 237.
24. Sedlar, M; Sayer, M; J. Sol-Gel Sci. and Technol., **1995**, 5, 27.
25. Schubert, U; J. Sol-Gel Sci. Technol., **2015**, DOI 10.1007/s10971-015-3920-0
26. Bradley, D.C; Mehrotra, R.C; Gaur, D.P; Metal Alkoxides, Academic Press, New York, **1978**.
27. Dunuwila, D.D; Gagliardi, C.D; Berglund, K.A; Chem. Mater., **1994**, 6, 1556.
28. Choi, H; Stathatos, E; Dionysiou, D.D; Appl. Catal. B: Environ., **2006**, 63, 60.
29. Kos´cielska, B; Winiarski, A; J Non-Crystalline Solids, **2008**, 354, 4349.
30. Wang, M.C; Lin, C.H; Wang, H.C; Wu, Ceramics Inter., **2012**, 38, 195.
31. Asahi, R; Morikawa, T; Ohwaki, T; Aoki, K; Taga, Y; Science, **2001**, 293, 269.
32. Chen, X; Yu, P.Y; Mao, S.S; Science, **2011**, 331, 746.
33. Khan, M.U; Al-shahry, M; Ingler Jr, W.B; Science, **2002**, 297, 2243.
34. Yu, J; Dai, G; Xiang, Q; Jaroniec, M; J. Mater. Chem., **2011**, 21, 1049.
35. Lin, Y; Jiang, Z; Zhu, C; Hu, X; Zhang, X; Zhu, H; Fan, J; Lin, S.H; J. Mater. Chem. A, **2013**, 1, 4516.
36. Danish, M; Pandey, A; J Mater Sci: Mater Electron. **2016,** 27, 6939.
37. JCPDS-PDFS, Jpn. J. Appl. Phys., **1965** 4, 8.
38. JCPDS-PDFS, Inorganic Volume, **1967** 6-10, 7.
39. Pankove, I; Optical Processes in Semiconductors. Englewood Cliffs NJ, Prentice-Hall, **1971**.
40. Gaya, U.I; Abdullah, A.H; J. Photochem Photobiol C Photochem Rev., **2008**, 9, 1.
41. Akpan, U.G; Hameed, B.H; J. Hazardous Mat., **2009**, 170, 520.

